

**Basics of lava-lamp convection**Balázs Gyüre<sup>1</sup> and Imre M. Jánosi<sup>1,2</sup><sup>1</sup>*von Kármán Laboratory of Environmental Flows, Loránd Eötvös University, Pázmány P. s. 1/A, H-1117 Budapest, Hungary*<sup>2</sup>*Institute for Mathematics and its Applications, University of Minnesota, 400 Lind Hall, 207 Church Street SE, Minneapolis, Minnesota 55455, USA*

(Received 9 April 2009; published 8 October 2009)

Laboratory experiments are reported in an immiscible two-fluid system, where thermal convection is initiated by heating at the bottom and cooling at the top. The lava-lamp regime is characterized by a robust periodic exchange process where warm blobs rise from the bottom, attach to the top surface for a while, then cold blobs sink down again. Immiscibility allows to reach real steady (dynamical equilibrium) states which can be sustained for several days. Two modes of lava-lamp convection could be identified by recording and evaluating temperature time series at the bottom and at the top of the container: a “slow” mode is determined by an effective heat transport speed at a given temperature gradient, while a second mode of constant periodicity is viscosity limited. Contrasting of laboratory and geophysical observations yields the conclusion that the frequently suggested lava-lamp analogy fails for the accepted models of mantle convection.

DOI: [10.1103/PhysRevE.80.046307](https://doi.org/10.1103/PhysRevE.80.046307)

PACS number(s): 47.55.pb, 44.25.+f, 91.45.Fj

**I. INTRODUCTION**

The “lava lamp” is a commonly known widget typically used for decoration. Its prototype was invented by Walker after World War II, but it has been mass marketed only since the sixties [1]. The most essential ingredients are two immiscible fluids of densities and thermal expansion coefficients such that they can be operated in a temperature range where the densities cross. The mixture is heated from below and freely cools at the top of its hermetically sealed container, such that the temperature gradient initiates heterogeneous thermal convection. The patterns formed by the randomly shaped blobs of the opaque component might be reminiscent of lava flow, hence the name.

Besides its decorative function, the lava lamp has been used also as visual aid in geoscience courses [2] demonstrating phenomena such as the transformation of energy, force and motion, adiabatic circulations in the atmosphere and oceans, or magma convection contributing to global plate tectonics. Indeed, the lava-lamp analogy has appeared in editorials of Science Magazine [3,4] and Nature [5], and in several research papers [6–9]. Although hundreds of recipes are accessible on the web, information on the physics of lava lamp such as heterogeneous thermal convection is hardly available in the literature, to our best knowledge.

Laboratory models have proved to be a useful exploratory tool in the context of mantle convection, too. Motivated by the ample evidences of large-scale mantle heterogeneity and its stratified structure [10], a number of studies have been performed in two layers of *immiscible* fluids [11–15] as a generalization of the fundamental one-layer Rayleigh-Bénard convection. The two-layer-convection problem has a rather high-dimensional parameter space (an order of ten nondimensional parameters may be important), but only a very small region is accessible in laboratory models. For this very reason, such phenomena as various interface deformations, wavy pattern formation, or oscillatory modes of coupled convection in the layers are widely studied; however, none of the experiments known to us has “driven” the parameters into the regime of lava-lamp convection.

In spite of the remarkable heterogeneities of the mantle, mixing processes obviously have played an important role in the formation of Earth’s present structure [16]. Inspired by this fact, many experiments have been designed on thermal convection in two layers of *miscible* fluids [17–26]. The initial stratification of various common solutions (glycerol, salt, cellulose, different syrups, etc.) decays rather quickly after thermal convection sets in; therefore, the main difficulties are to collect enough data and interpret them in a continually changing transient state of the system. Nevertheless, models of miscible fluids eliminate side effects of chemical incompatibilities such as interfacial tension, which is considered to be irrelevant in the mantle [10,27].

In this work we report on experiments in a two-layer immiscible fluid system driven into the “lava-lamp convection” regime, where warm blobs ascend from the bottom and cold blobs descend from the top periodically. The primary goal was to construct a robust setup which is dependably reproducible, chemically neutral, and thermally stable; therefore, the measurement technique is rather simple by recording time series of the bottom and top temperatures. Still we could identify two main modes of lava-lamp convection. At moderate temperature gradients, an effective heat transport speed determines the frequency of blob rising and sinking cycle. This frequency tends to be a constant value at large enough temperature contrasts indicating that viscosity becomes the governing factor. In Sec. II C we discuss quantitative aspects of the regular oscillations, while Sec. III is devoted to summarize the limitations of an analogy with mantle convection.

**II. EXPERIMENTS**

The laboratory lava-lamp setup is shown in Fig. 1; the construction is almost trivial. There are a few details which might help to reproduce the experiments. First, the metal lid at the top has a rubber stuffing along the fringe to minimize evaporative loss. Second, the shape of the lid is not flat; the cross section in Fig. 1 (part C) indicates the thermal dilata-

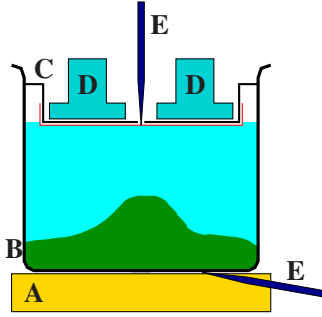


FIG. 1. (Color online) Sketch of the experimental setup. A: regulated heating block, B: cylindrical glass container (diameter  $D=25.0$  cm), C: thin metal lid with plastic envelope, D: copper cooling ring of circulated water, and E: Ni-NiCr thermocouples. The filling is heavy silicone oil and salt solution (see text).

tion volume around the inner perimeter of the glass container. Third, a proper cleaning of the internal glass surface (and the lid) is very essential because invisible microscopic depositions can easily pin the silicone oil (see below) blobs to the walls. For the same reason, the bottom of the metal lid was covered by a thin refractory plastic foil of nonadhesive outer surface (shown without a separate label in Fig. 1).

Both the heating and cooling blocks were regulated by circulating water. Temperatures were measured by Ni-NiCr thermocouples (diameter 0.5 mm) touching the outer surfaces of the container at the top and also at the bottom. (As Fig. 1 depicts, the upper metal lid has a hole in the middle; thus, the temperature sensor hits the plastic foil.) The measured temperature values represent averages over extended volumes, but this was purposeful: apart from the fact that the thermocouple wires pin the blobs when they immersed into the tank, the presented experiments did not aim to resolve local temperature fluctuations. Measured values in every 5 s were recorded. A typical experimental run at fixed boundary temperatures lasted approximately 24 h; the longest continuous measurement was sustained for 2 weeks without any problem.

The temperature sensor at the bottom of the container was not connected to the heating thermostat; a separate sensor was installed for control purposes. Since our goal was to construct a first working setup, and we intended to follow the processes by continuous visual inspection, no sidewall thermal insulation was installed. (Note that commercial lava lamps function well without thermal insulation.)

### A. Fluid properties and parameters

The first component we found to be appropriate is a heavy silicone fluid [poly(dimethyl-methyl-phenyl-siloxane)] available under the brand name Wacker AP 500. A few essential material parameters are reproduced from the product data sheet in Table I, as well as for the second fluid component, the common salt solution (NaCl in distilled water). The latter has the advantage that its density can be easily fine tuned without appreciably changing its thermal expansion properties.

The most important attribute of an immiscible two-fluid system where lava-lamp convection expected is that the two

TABLE I. Physical properties (reference values for 25 °C) of the NaCl solution, silicone oil (Wacker AP 500), and the liquid mantle [10]. (The Rayleigh number  $Ra=\alpha g \Delta T H^3 / \nu \kappa$  is estimated for the NaCl solution and silicone oil assuming a homogeneous filling height of  $H=30$  cm and temperature contrast  $\Delta T=20$  K.)

Quantity	NaCl solution	Silicone fluid	Mantle
$\rho$ (kg/m <sup>3</sup> )	1074	1080	3250–3600
$\mu$ (Pa s)	$1.08 \times 10^{-3}$	0.475–0.525	$10^{21}$
$\nu = \frac{\mu}{\rho}$ (m <sup>2</sup> /s)	$1.0 \times 10^{-6}$	$440\text{--}486 \times 10^{-6}$	$3 \times 10^{17}$
$c_p$ (J kg <sup>-1</sup> K <sup>-1</sup> )	3993	1591	1250
$k$ (W m <sup>-1</sup> K <sup>-1</sup> )	0.596	0.146	3.3
$\kappa = \frac{k}{\rho c_p}$ (m <sup>2</sup> /s)	$1.4 \times 10^{-7}$	$0.85 \times 10^{-7}$	$0.8\text{--}3 \times 10^{-6}$
$Pr = \frac{\nu}{\kappa}$	7	5400	$10^{23}$
$\alpha$ ( $\times 10^{-6}$ K <sup>-1</sup> )	280	470	10–40
Ra	$\sim 10^9$	$\sim 10^7$	$10^7\text{--}10^9$

density-temperature curves must intercept each other, possibly not very far from room temperature. This condition is fulfilled in our mixture as illustrated in Fig. 2. The gray curve is one of the widely used empirical approximations for the temperature dependence of the density of salt solution [28] showing the reliability of our own measurements; nevertheless, a simple cubic polynomial fit works equally well in the given temperature range. It is clear that the linear approximation for the thermal expansion coefficient  $\alpha$  in Table I is valid only for the initial part of the curves.

When the filling materials and the diameter of the container are fixed as in our case ( $D=25.0$  cm), the control variables of the setup are the volume of the silicone oil  $V_{oil}$  and the salt solution  $V_{ss}$ , furthermore, the average temperatures at the heated bottom  $T_w$  and at the cooled top  $T_c$ . For the sake of subsequent comparisons, the parameters are expressed as nondimensional ratios: the aspect ratio  $r_a=H/D$  of the filling height  $H$  and diameter  $D$ , the volumetric ratio  $r_v=V_{oil}/V_{ss}$ , and the relative temperature contrast  $r_T=(T_w-T_c)/T_w$ . The temperatures are determined in units of Kelvin; thus,  $r_T$  has very low numerical values for the ex-

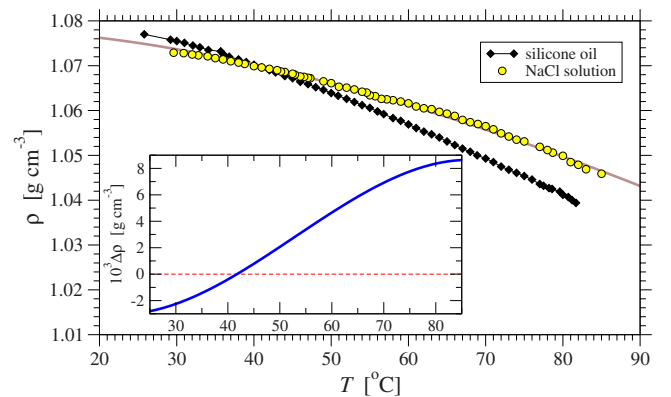


FIG. 2. (Color online) Fluid densities as a function of temperature. Light symbols: Wacker AP 500 silicone oil; black symbols: salt solution (100.654 g/kg NaCl in distilled water). The dark gray line illustrates a commonly used empirical formula [28]. The inset shows the density difference as a function temperature.

periments, nevertheless, it helps at discussing the mantle analogy. Note that we do not adopt the usual control parameter of convection experiments, the Rayleigh number  $Ra = \alpha g(T_w - T_c)H^3 / \nu \kappa$ , because we could not find any reasonable way to combine somehow the differing material parameters of the two fluids especially for the lava-lamp convection regime.

An important parameter relating the stable “chemical” density contrast  $\Delta \rho$  (at a fixed temperature) to the unstable “thermal” density difference is the buoyancy number [29], which is expressed usually as  $B = \Delta \rho / \rho \alpha \Delta T$ , where  $\alpha$  is an “average” thermal expansion coefficient. Figure 2 illustrates that an assumption of linear thermal expansion provides a very poor approximation; therefore, we introduce a more accurate buoyancy number as

$$B_{oil} = \frac{\rho_{oil}(T_c) - \rho_{ss}(T_c)}{\rho_{oil}(T_c) - \rho_{oil}(T_w)}, \quad (1)$$

where the index of  $B$  refers to the denominator and the densities are determined from the measured values at each temperature point. Nevertheless, this number remains a very approximate parameter of the system because the actual buoyancy forces are determined by a strongly inhomogeneous and continuously changing temperature field inside the fluid. Note also that  $r_T$  and  $B$  are not entirely independent; in case of a strictly linear density-temperature behavior they would obey a strict inverse relationship.

### B. Convective behavior

The first observation is that the general final state of the two-fluid system with “randomly” chosen volumetric ratios and temperature contrasts is a stationary configuration; a few examples are shown in Fig. 3. Depending on subtle details, the two components split up into two regions, where both fluids can span from bottom to top, or the component of smaller volume remains stuck either on the top or on the bottom (see Fig. 3). The fluids in both compartments exhibit thermal convection of sometimes complicated internal flow patterns; subsequent experiments will expose the details. The lack of thermal insulation along the vertical wall certainly perturbed the flow fields; however, external temperature measurements suggested that the total heat loss could not be higher than a few percent [30].

Fine tuning was necessary to reach the lava-lamp convection regime. When the volumetric ratio of the components and the temperature contrast are properly chosen, the thermal convection manifests as a periodic exchange process shown in Fig. 4. Figure 4(a) illustrates a configuration where a layer of the silicone fluid covers the bottom of the container. Since most of the heat is absorbed by this component, the temperature begins to increase until the density drops to a critical level. At this stage, a rising blob forms which breaks away and sticks to the top [Fig. 4(c)]. The enhanced heat loss at the top promotes the formation of a large-density blob which eventually sinks to the bottom [Fig. 4(f)] and a new cycle begins.

Figure 5 illustrates typical temperature records of the sensors. The main characteristic is the marked asymmetric

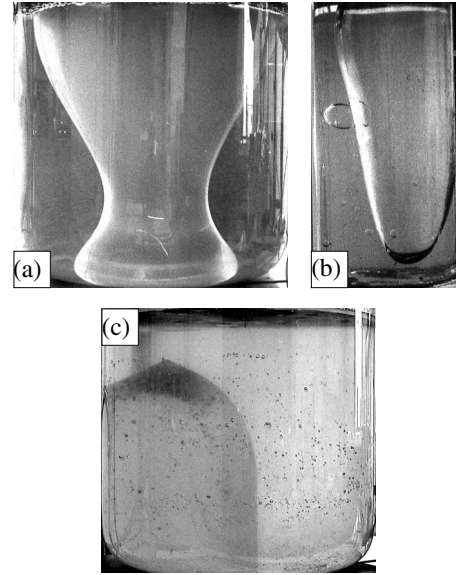


FIG. 3. Stationary configurations at different aspect ratios  $r_a = H/D$ , fluid volume ratios  $r_V = V_{oil}/V_{ss}$ , and relative temperature contrasts  $r_T = (T_w - T_c)/T_w$  (values in units of Kelvin). (a)  $r_a = 0.96$ ,  $r_V = 0.60$ , and  $r_T = 0.066$ ; (b)  $r_a = 1.70$ ,  $r_V = 0.23$ , and  $r_T = 0.078$ ; (c)  $r_a = 0.84$ ,  $r_V = 0.41$ , and  $r_T = 0.051$ . The more opaque component is the silicone fluid in each snapshot.

warming-cooling periodicity at the top. The local temperature extremes do not coincide with the conspicuous dynamical events shown in Fig. 4. This is because both fluids have strong thermal inhomogeneities and intense internal convection proceeds together with the blob-exchange dynamics resulting in delays for the temperature signals.

It is remarkable that the system is very sensitive to fine details. Figure 6 illustrates an attempt to separate the parameters for lava-lamp convection. (The incorporation of the as-

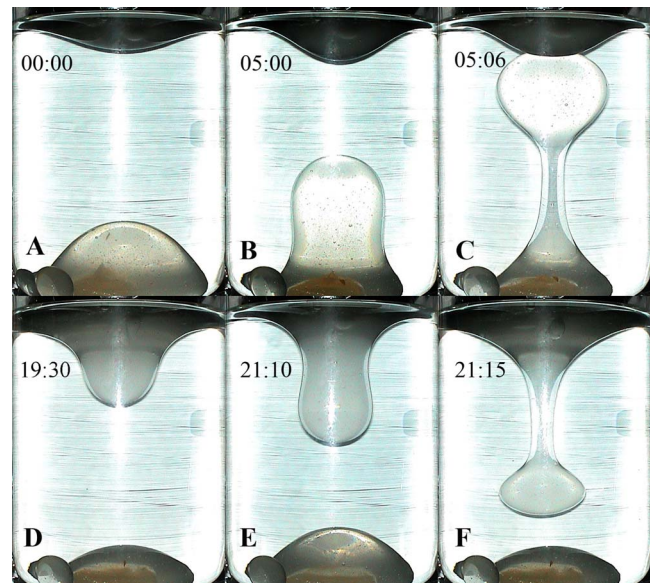


FIG. 4. (Color online) Lava-lamp convection at parameter values  $r_a = 1.12$ ,  $r_V = 0.21$ , and  $r_T = 0.060$ ; relative time is indicated (minutes:seconds).

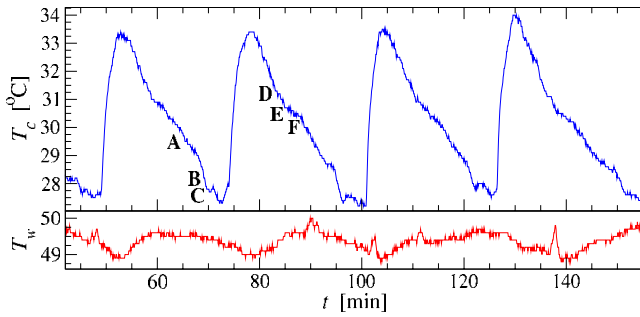


FIG. 5. (Color online) Temperature records determined with a temporal resolution of 5 s with the sensors depicted in Fig. 1:  $T_c$  at the top and  $T_w$  at the bottom. Labels A–F identify the time moments when the snapshots in Fig. 4 were taken.

pect ratio does not improve the picture partly because most of the experiments were performed in setups  $r_a \in [1.0; 1.3]$ .) The overlap of the different symbols demonstrates that the external parameters alone cannot guarantee a robust lava-lamp convection. Most probably microscopic details are crucial such as contaminations in the fluids and on the surfaces which are very difficult to control. Note also that the silicone fluid itself represents an element of uncertainty because its

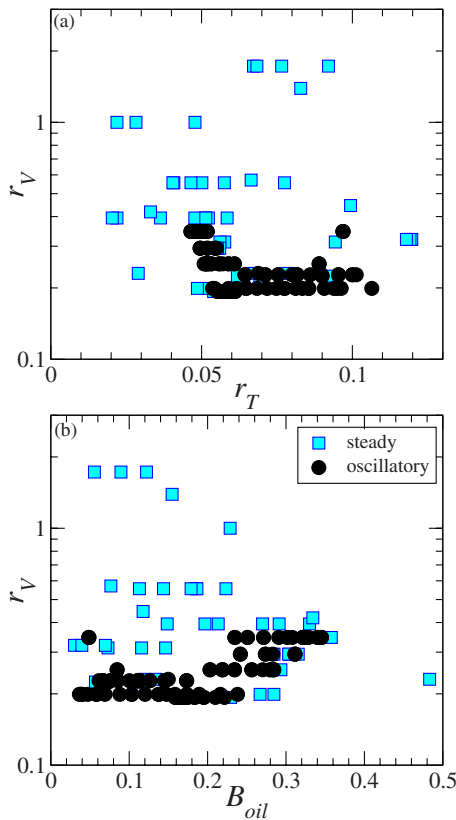


FIG. 6. (Color online) Tested parameter space region of the experiments. Stable oscillatory mode was established only after 24 h of continuous operation without any intermission. (a) Control parameters are the relative temperature contrast  $r_T = (T_w - T_c) / T_w$  (values are in units of Kelvin) and the fluid volume ratio  $r_V = V_{oil} / V_{ss}$ . (The vertical scale is logarithmic.) (b) The same as above with  $B_{oil}$  on the horizontal axis [see Eq. (1)].

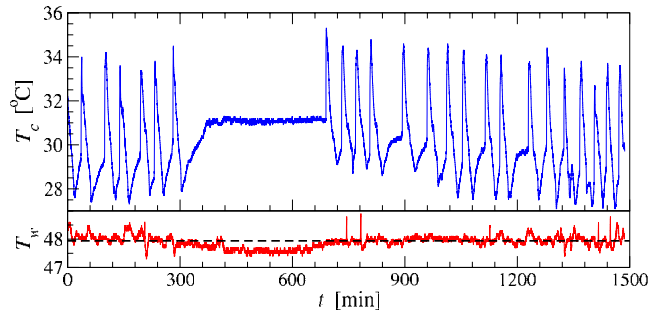


FIG. 7. (Color online) Reversible switch of oscillatory convection by a slight tuning of the bottom control temperature.  $r_a = 1.12$ ,  $r_V = 0.22$ , and  $r_T = 0.055$ .

precise chemical composition is not entirely fixed. (Fractions of different polymer chain lengths have different densities, which can contribute to the permanent oil layers both at the top and the bottom visible in Fig. 4.) On the other hand, when lava-lamp convection sets in at appropriate parameters (heavy circles in Fig. 6), it remains stable and reversible.

**C. Properties of the thermal oscillations**

The reversible nature of the lava-lamp convection is demonstrated in Fig. 7. A moderate decrease ( $\sim 0.5^\circ\text{C}$ ) of the bottom control temperature resulted in a break off for blob-exchange processes; however, the return switched on the original mode again. This reversibility is not restricted to slight temperature changes; a setup tuned into the lava-lamp regime remains stable and reproduces all aspects of convection after weeks of intermissions. (Actually, lava-lamp widgets could not be commercialized in the absence of such stability.)

The magnitude of the bottom control temperature is limited by the fact that hot water was circulated in the heating block. In the available interval, the generic lava-lamp dynamics was the “single-blob-exchange” convection illustrated in Figs. 4 and 5. In a few cases, however, the convection cycle exhibited a more complex pattern consisting of two smaller successive hot blobs rising from the bottom and a single sinking one from the top. The characteristic temperature signal for such mode is plotted in Fig. 8. This mode evolved spontaneously from the single-blob-exchange convection without external control; therefore, its reproducibility

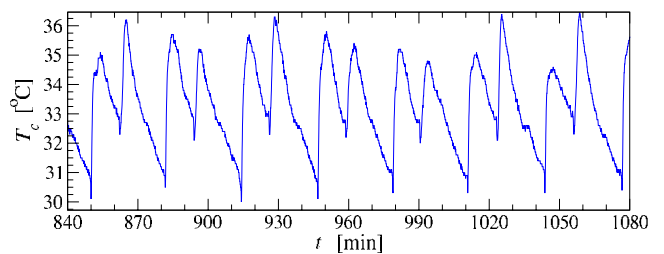


FIG. 8. (Color online) Dual sawtooth temperature oscillations recorded at the top. In this mode, two smaller consecutive rising drops and a single sinking ball constitute one cycle of the periodic convection.  $r_a = 1.12$ ,  $r_V = 0.22$ , and  $r_T = 0.061$ .

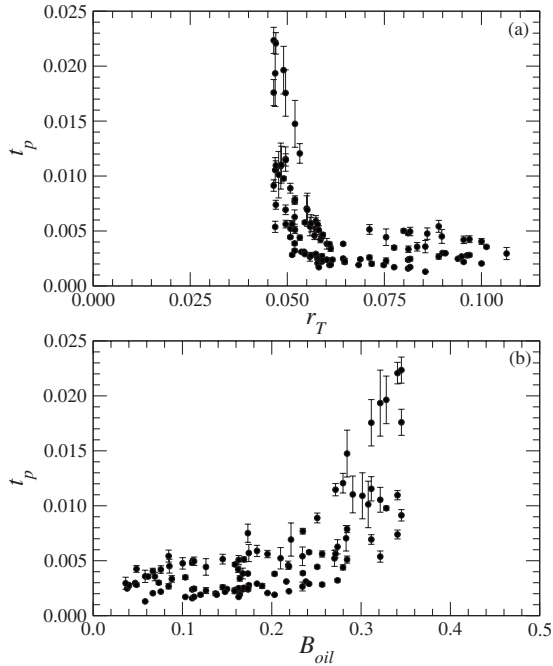


FIG. 9. (a) Nondimensional time period  $t_p$  (see text) as a function of relative temperature contrast  $r_T$  for the experiments in the oscillatory convection regime. Vertical error bars were obtained from the half-width of Fourier peaks around the characteristic frequencies  $t_p^{-1}$ . (b) The same as (a) as a function of buoyancy number  $B_{oil}$ .

remained quite weak. Nevertheless, the existence of this convective mode is an important indication to the essential role of nonlinearities in the system. Fully developed chaotic dynamics of several randomly shaped blobs, which is the well-known specialty of commercial widgets, was not found in our experiments.

An obvious quantity to extract from oscillatory signals is the characteristic time period and its dependence on the control parameters. The period for a given time series was determined by Fourier transformation; the location and width of the main peak allowed estimation of an average value and error. A convenient way to define a nondimensional time period is based on the normalization by an intrinsic time scale, the vertical thermal diffusion time  $\tau = H^2/\kappa$ , where  $H$  is the total fluid height and  $\kappa$  is the thermal diffusivity. Unlike an effective Rayleigh number,  $\tau$  is not connected to convection; thus, it can be easily estimated for a composite system as  $\tau = h_{oil}^2/\kappa_{oil} + h_{ss}^2/\kappa_{ss}$ , where  $H = h_{oil} + h_{ss}$ , and the indices denote parameters for the silicone oil and salt solution, respectively. In our experiments, values in the range  $\tau \approx 2-5$  days were typical. The nondimensional time period  $t_p$  is plotted as a function of the nondimensional temperature contrast ratio  $r_T$  as well as the buoyancy number  $B_{oil}$  in Fig. 9.

The first observation is that blob-exchange oscillations require a minimum thermal driving; an apparent threshold value is around  $r_T \approx 0.045$  for the fluids in our system. The corresponding buoyancy number is around  $B_{oil} \approx 0.36$ . The oscillation period steeply drops for stronger temperature contrasts. In this regime, the governing factor is presumably an

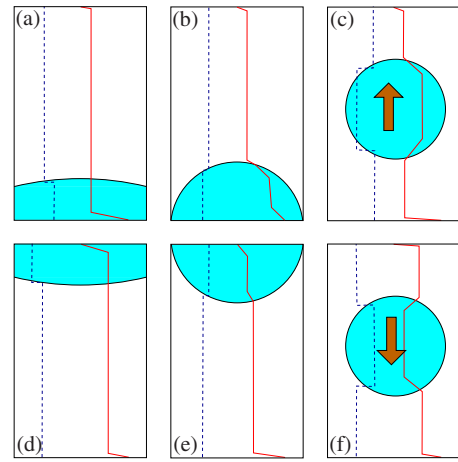


FIG. 10. (Color online) Sketch of the stages of blob-exchange oscillations, approximate density, and temperature profiles are indicated by dashed (blue) and solid (red) lines. (a) Initial warming up. (b) Near blob formation, where the densities are almost equal. (c) An overheated blob of decreased density rises up. (d) Cooling of the blob material. (e) Near blob formation at the top. (f) A cold blob of increased density sinks down.

effective heat transfer speed determining the warming time for critical buoyancy in the bottom layer. (The effective heat transfer speed can be considered as the average value of the fluctuating heat flux across the bottom boundary.) In agreement with the physical intuition, the oscillation period  $t_p$  does not converge to zero; it saturates around  $t_p \approx 0.003 \pm 0.001$  for  $r_T > 0.06$  ( $B_{oil} < 0.2$ ). Here the limiting factor is most probably the viscosity of the silicone fluid moderating the internal convection in the layer which determines the hot blob formation.

#### D. Qualitative explanation

The full hydrodynamic description of thermal convection in a two-fluid system is overly complicated by the mutual influence of the flow and the interfacial deformation; therefore, only numerical methods are conceivable. In the case of very strong deformations and especially under conditions of an interfacial breakup, the adaptation of the computational grid to the moving interface becomes a difficult task [15]. Since the treatment of such problem is beyond our capabilities, here we settle for a qualitative formulation of the basic physics behind the blob-exchange oscillations.

Figure 10 illustrates the phases of blob-exchange flow in an idealized situation. Direct observations indicate that both fluids exhibit vigorous thermal convection; therefore, we assume that the internal temperature profiles are similar to a single fluid arrangement with more or less constant values apart from the thermal boundary layers. Since the viscosities and thermal conductivities are rather different (see Table I), the temperatures can have different average values in the two fluids for a while. The key factor for blob-exchange convection is the crossing of the density-temperature curves shown in Fig. 2. Such crossing guarantees that two stable isothermal layering configurations exist as a function of temperature. This is essential because thermal convection tends to homog-

enize the temperature inside the volume. At the beginning, the silicone oil has higher density than the salt water [Fig. 10(a)]. When a temperature difference builds up, the density difference diminishes [Fig. 10(b)] and it can change sign. Large enough density drop inside the silicone oil allows the formation of a rising blob [Fig. 10(c)]. The higher temperature inside the blob results in the periodic “heat shocks” at the top clearly indicated by the time series in Figs. 5, 7, and 8. When the oil blob layers at the top [Fig. 10(d)], the process reverses. The cooling of the oil is slower than the warming of water; therefore, the temperature contrast changes sign again [Fig. 10(e)] until a sinking blob of large density forms [Fig. 10(f)]. Note that the periodic temperature drop at the bottom is clearly visible in Fig. 5; the smaller amplitude is due to the fact that the bottom sensor is directly attached to the heating block (see Fig. 1).

### III. DISCUSSION: FAILURE OF THE MANTLE ANALOGY

Although several details will be explored in subsequent experiments with more advanced measuring methods, we can discuss where the analogy with mantle convection probably holds or fails. The first obvious departure from the widely accepted picture of mantle convection is the opposing viscosity ratio between the hot rising blobs and surrounding fluid. The initial viscosity of the silicone fluid ( $\mu \approx 0.5$  Pa s at 25 °C; see Table I) drops almost exponentially ( $\mu \approx 0.05$  Pa s at 80 °C [31,32]), still its value remains two orders of magnitude higher than that is for the salt solution [33]. Contrarily, model studies suggest a factor of 100 *reduction* in viscosity inside a rising mantle plume [34]. On the other hand, neutrally buoyant isolated blobs of higher internal viscosities have been proposed to explain long-lived chemical heterogeneities in the mantle [35,36] because an increased blob viscosity may prevent from mixing with the surrounding material. This hypothesis has been questioned in recent studies [37,38]; nevertheless, the lava-lamp setup is certainly a model system for hot blobs of high viscosity.

The second essential difference from the convecting mantle is the immiscibility of the fluids in the model. Although recent works report on a high degree of upper-mantle chemical heterogeneity [39–41], its extent is far less than for an oil-water system. Obviously the laboratory model is set for investigating dynamical aspects of two-fluid thermal convection and not for mixing.

The most serious problem is an unavoidable side effect of chemical incompatibility: the emergence of interfacial tension. Measured values for the polysiloxane-water systems are around  $\gamma \approx 40$  mN/m at 20 °C [42]. Its dynamical importance is usually estimated by the Bond number [15],

$$\text{Bo} = \frac{\Delta \rho g L^2}{\gamma},$$

where  $L$  is a characteristic length scale of the problem (usually a layer depth). Irrespective of the magnitude of  $\gamma$ , it is obvious the Bo can be arbitrarily small, since the density-

temperature curves cross each other (Fig. 2) with  $\Delta \rho = 0$ . This entails that the interfacial tension is the determining factor at some stage of the dynamics of blob formation. For example, it is possible that the apparently spontaneous switches to the two-rising-blob mode (see Fig. 8) are determined by the interfacial tension (together with viscosity effects).

Simple direct observations also support that the presence of interfacial tension decisively affects the dynamics. One of the standard procedures to estimate  $\gamma$  is the “breaking thread method” [43], where long liquid threads in a different fluid exhibit sinusoidal distortions which cause them to break up into a number of small droplets. During lava-lamp convection, such cylindrical threads periodically evolve in each blob-exchange cycle [see Figs. 4(c) and 4(e)] and small droplet formation regularly occurs. Such a secondary droplet is clearly visible in Fig. 4 at the bottom-left corner. A quantitative estimate for  $\gamma$  is not possible by measuring the size of these blobs because the shear along the threads is far from being negligible [43].

Finally, it is worth to have a closer look at the thermal oscillations discussed in Sec. II C. Periodic time evolution of temperature signals close to both horizontal boundaries is a prevalent behavior in similar systems. It appears in chemically homogeneous fluids of temperature-dependent viscosities [44] or in two-layer miscible liquids [20,24] and it is predicted by several numerical simulations [45–47]. Seismology provides a snapshot of the Earth’s structure with clear evidence for stratification in the mantle; however, a strict layering at 660 km depth can be ruled out based on dynamical considerations alone and the preferred form remains a moderated whole mantle convection [6,16,48]. This entails that the relative temperature contrast can be estimated around  $r_T \approx 0.8–0.9$ , far beyond the accessible range of laboratory experiments. The thermal diffusion time across the mantle is on the order of  $\tau \approx 1.2 \times 10^{11}$  yr (note that the age of the Earth is around  $4.54 \times 10^9$  yr). Just to toy with the idea that the time period of regular oscillations shown in Fig. 9 remains constant at very high temperature contrasts, this would give an estimated value  $t_p \approx 3–4 \times 10^8$  yr for whole-mantle convection. The same approximation gives  $t_p \approx 20$  million years for the assumption that hot blobs originate from a depth of the 660 km discontinuity. Rather surprisingly, Mjelde and Faleide have recently found a clear periodicity in the variation of Icelandic and Hawaiian magmatism with a characteristic time of ca. 15 million years [49]. Their results indicate also a “copulsation” of mantle plumes at the two regions, which they interpret as a sign of periodic heating of the earth’s core and a periodic increase in global plume activity. Our experiments suggest that a periodic heat release in heterogeneous thermal convection does not necessarily require a periodic heating mechanism.

### ACKNOWLEDGMENTS

This work was supported by the Hungarian Science Foundation (OTKA) under Grant No. NK72037.

- [1] K. K. Karukstis and G. R. Van Hecke, *Chemistry Connections: The Chemical Basis of Everyday Phenomena*, 2nd ed. (Academic, San Diego, 2003), p. 14.
- [2] S. G. Tolley and S. Richmond, *J. Geosci. Educ.* **51**, 217 (2003).
- [3] R. A. Kerr, *Science* **283**, 1826 (1999).
- [4] R. A. Kerr, *Science* **292**, 841 (2001).
- [5] M. McNutt, *Nature (London)* **402**, 739 (1999).
- [6] D. Bercovici and S. Karato, *Nature (London)* **425**, 39 (2003).
- [7] U. Hansen and D. A. Yuen, *Earth Planet. Sci. Lett.* **176**, 401 (2000).
- [8] B. Schott and D. A. Yuen, *Phys. Earth Planet. Inter.* **146**, 139 (2004).
- [9] N. H. Sleep, *Earth Sci. Rev.* **77**, 231 (2006).
- [10] G. Schubert, D. L. Turcotte, and P. Olson, *Mantle Convection in the Earth and Planets* (Cambridge University Press, Cambridge, 2001).
- [11] S. Rasenat, F. H. Busse, and I. Rehberg, *J. Fluid Mech.* **199**, 519 (1989).
- [12] P. Cardin and H. Nataf, *Europhys. Lett.* **14**, 655 (1991).
- [13] A. Prakash, K. Yasuda, F. Otsubo, K. Kuwahara, and T. Doi, *Exp. Fluids* **23**, 252 (1997).
- [14] M. M. Degen, P. W. Colovas, and C. D. Andereck, *Phys. Rev. E* **57**, 6647 (1998).
- [15] A. Nepomnyashchy, I. Simanovskii, and J. Legros, *Interfacial Convection in Multilayer Systems* (Springer, New York, 2006).
- [16] P. E. van Keken, E. H. Hauri, and C. J. Ballentine, *Annu. Rev. Earth Planet. Sci.* **30**, 493 (2002).
- [17] F. M. Richter and D. P. McKenzie, *J. Geophys. Res.* **86**, 6133 (1981).
- [18] P. Olson and C. Kincaid, *J. Geophys. Res.* **96**, 4347 (1991).
- [19] A. Davaille, *Nature (London)* **402**, 756 (1999).
- [20] A. Davaille, *J. Fluid Mech.* **379**, 223 (1999).
- [21] A. M. Jellinek, A. C. Kerr, and R. W. Griffiths, *J. Geophys. Res., [Solid Earth]* **104**, 7183 (1999).
- [22] A. Davaille, F. Girard, and M. Le Bars, *Earth Planet. Sci. Lett.* **203**, 621 (2002).
- [23] A. Davaille, M. Le Bars, and C. Carbonne, *C. R. Geosci.* **335**, 141 (2003).
- [24] M. Le Bars and A. Davaille, *J. Geophys. Res.* **109**, B03403 (2004).
- [25] C. Jaupart, P. Molnar, and E. Cottrell, *J. Fluid Mech.* **572**, 433 (2007).
- [26] I. Kumagai, A. Davaille, and K. Kurita, *Earth Planet. Sci. Lett.* **254**, 180 (2007).
- [27] D. L. Anderson, *Science* **293**, 2016 (2001).
- [28] S. C. McCutcheon, J. L. Martin, and T. O. Barnwell, in *Handbook of Hydrology*, edited by D. R. Maidment (McGraw-Hill, New York, 1993), p. 11.3–11.73.
- [29] F. M. Richter and C. E. Johnson, *J. Geophys. Res.* **79**, 1635 (1974).
- [30] C. Lithgow-Bertelloni, M. A. Richards, C. P. Conrad, and R. W. Griffiths, *J. Fluid Mech.* **434**, 1 (2001).
- [31] E. V. Zolotykh, D. I. Kuznetsov, and A. N. Krupina, *J. Eng. Phys. Thermophys.* **29**, 1163 (1975).
- [32] *CRC Handbook of Lubrication: Theory and Practice of Tribology*, edited by E. R. Booser (CRC Press, New York, 1989).
- [33] *Handbook of Water Analysis*, 2nd ed., edited by L. M. L. Nollet (CRC Press, New York, 2007).
- [34] A. M. Jellinek and M. Manga, *Rev. Geophys.* **42**, RG3002 (2004).
- [35] M. Manga, *Geophys. Res. Lett.* **23**, 403 (1996).
- [36] T. W. Becker, J. B. Kellogg, and R. J. O'Connell, *Earth Planet. Sci. Lett.* **171**, 351 (1999).
- [37] J. B. Naliboff and L. H. Kellogg, *Phys. Earth Planet. Inter.* **161**, 86 (2007).
- [38] J. Schneider, J. Schmalzl, and T. Tél, *Chaos* **17**, 033115 (2007).
- [39] A. Luguét, D. G. Pearson, G. M. Nowell, S. T. Dreher, J. A. Coggon, Z. V. Spetsius, and S. W. Parman, *Science* **319**, 453 (2008).
- [40] A. Meibom, *Science* **319**, 418 (2008).
- [41] T. Plank and P. E. van Keken, *Nature Geosci.* **1**, 17 (2008).
- [42] H. W. Fox, P. W. Taylor, and W. A. Zisman, *Ind. Eng. Chem.* **39**, 1401 (1947).
- [43] P. H. M. Elemans, J. M. H. Janssen, and H. E. H. Meijer, *J. Rheol.* **34**, 1311 (1990).
- [44] N. Schaeffer and M. Manga, *Geophys. Res. Lett.* **28**, 455 (2001).
- [45] S. A. Weinstein, P. L. Olson, and D. A. Yuen, *Geophys. Astrophys. Fluid Dyn.* **47**, 157 (1989).
- [46] T. B. Larsen, D. A. Yuen, J. Moser, and B. Fornberg, *Geophys. Astrophys. Fluid Dyn.* **84**, 53 (1997).
- [47] P. Beltrame, V. Travníkov, M. Gellert, and C. Egbers, *Nonlinear Processes Geophys.* **13**, 413 (2006).
- [48] P. J. Tackley, *Science* **288**, 2002 (2000).
- [49] R. Mjølde and J. I. Faleide, *Mar. Geophys. Res.* **30**, 61 (2009).